

A New Well-Balanced Finite Volume CWENO Scheme for Shallow Water Equations over Bottom Topography

Wei Guo¹, Ziming Chen¹, Shouguo Qian^{1,*}, Gang Li^{1,*}
and Qiang Niu²

¹ School of Mathematics and Statistics, Qingdao University, Qingdao, Shandong 266071, China

² Department of Applied Mathematics, Xi'an Jiaotong-Liverpool University, Suzhou, Jiangsu 215123, China

Received 8 May 2022; Accepted (in revised version) 27 October 2022

Abstract. In this article, we develop a new well-balanced finite volume central weighted essentially non-oscillatory (CWENO) scheme for one- and two-dimensional shallow water equations over uneven bottom. The well-balanced property is of paramount importance in practical applications, where many studied phenomena can be regarded as small perturbations to the steady state. To achieve the well-balanced property, we construct numerical fluxes by means of a decomposition algorithm based on a novel equilibrium preserving reconstruction procedure and we avoid applying the traditional hydrostatic reconstruction technique accordingly. This decomposition algorithm also helps us realize a simple source term discretization. Both rigorous theoretical analysis and extensive numerical examples all verify that the proposed scheme maintains the well-balanced property exactly. Furthermore, extensive numerical results strongly suggest that the resulting scheme can accurately capture small perturbations to the steady state and keep the genuine high-order accuracy for smooth solutions at the same time.

AMS subject classifications: 74S10

Key words: Shallow water equations, source term, CWENO scheme, decomposition algorithm, well-balanced property.

1 Introduction

In this article, we concern with developing a high-order finite volume CWENO scheme for shallow water equations (SWEs), which in one-dimensional space enjoy the following

*Corresponding author.

Emails: 1161362621@qq.com (W. Guo), zimingchen123@163.com (Z. Chen), sgqian1976@163.com (S. Qian), gangli1978@qdu.edu.cn (G. Li), qiang.niu@xjtlu.edu.cn (Q. Niu)

form

$$h_t + (hu)_x = 0, \quad (1.1a)$$

$$(hu)_t + \left(hu^2 + \frac{1}{2}gh^2 \right)_x = -ghb_x. \quad (1.1b)$$

Here, $h(x,t)$, $u(x,t)$ and $b(x)$ represent the water depth, the depth-averaged velocity, and the bottom, respectively. The constant $g = 9.812$ denotes the gravitational constant. High order schemes solving SWEs enjoy the key role in fields of the hydraulic science and the coastal engineering [1–3].

The geometric source term on the right hand side of (1.1) is due to the uneven bottom topography. For conciseness, the system (1.1) can be rewritten as a compact vector form

$$U_t + F(U)_x = S(U,b), \quad (1.2)$$

with

$$U = (h, hu)^\top, \quad F(U) = \left(hu, hu^2 + \frac{1}{2}gh^2 \right)^\top \quad \text{and} \quad S(U,b) = (0, -ghb_x)^\top$$

being the vector of the conservative variable, the physical flux, and the source term, respectively. The system (1.1) keeps a subtle equilibrium between the flux gradient and the source term. From the mathematical point of view, the system (1.2) holds non-trivial steady state solutions that satisfy an ordinary differential equation (ODE)

$$F(U)_x = S(U,b).$$

Herein, we are interested in the still water steady state solutions as follows

$$u = 0, \quad h + b = \text{Constant}. \quad (1.3)$$

In general, the traditional schemes coupled with standard numerical fluxes as well as direct discretizations of the source term fail to maintain the above delicate equilibrium, and lead to non-physical oscillations especially near discontinuities, which will not disappear even on a very refined mesh.

Well-balanced schemes [4, 5] can preserve the steady state up to the machine accuracy at the discrete level and resolve small perturbations of the steady state even on a relatively coarse mesh [6], then increase the computational efficiency correspondingly. Following the original works [4, 5], many researchers have made extensive attempts in the development of well-balanced schemes. Representative researches mainly include: kinetic scheme [7], gas-kinetic scheme [8], central-upwind scheme [9], weighted essentially non-oscillatory (WENO) schemes [10–19], Hermite WENO scheme [20], central schemes [21, 22], Runge-Kutta discontinuous Galerkin (RKDG) methods [23–25], ADER (Arbitrary DERivatives in time and space) schemes [26, 27], spectral element method [28], Godunov-type method [29], element-free Galerkin method [30], ADER discontinuous

Galerkin (ADER-DG) method [31], and so on. The research on the well-balanced schemes has become a very popular subject. The latest progresses of this subject can be found in the book of Gosse [32]. For a historic review about this subject, we refer to [33, 34] for more details.

The key objective of this article is to develop a new well-balanced finite volume CWENO scheme by means of a novel full equilibrium preserving reconstruction procedure. This type of reconstruction procedure can lead to a decomposition algorithm, which helps us construct well-balanced numerical fluxes and achieve a simple source term discretization easily.

Specifically, during the process of constructing numerical fluxes at inter-cells, we are free of using the traditional hydrostatic reconstruction technique [35]. The hydrostatic reconstruction technique [35] is often applied to construct well-balanced numerical fluxes [19, 24, 25, 31].

In addition, for the source term discretization, the resulting scheme only uses simple Gaussian quadrature rules and avoids using complex source term splitting. Compared with the traditional WENO reconstruction in [36, 37], the linear weights of the CWENO reconstruction are not needed to guarantee the accuracy of the reconstruction in smooth regions and can be chosen rather arbitrarily. Moreover, all the nonlinear weights involved in the CWENO reconstruction do not depend on particular points. Particularly, the CWENO reconstruction here is especially suitable for finite volume schemes with respect to hyperbolic balance laws such as SWEs (1.1), where high-order quadrature rules using several points are needed for the cell averages of the source term.

This article is organized as follows: In Section 2, we present well-balanced finite volume CWENO schemes for one-dimensional SWEs. Subsequently, we extend the proposed scheme to two-dimensional system in Section 3. In Section 4, we implement extensive numerical examples to demonstrate the performance of the resulting scheme. Finally, some conclusions are drawn in Section 5.

2 Construction of well-balanced finite volume CWENO scheme for one-dimensional problems

In this section, we concentrate on construction of the well-balanced finite volume CWENO scheme for one-dimensional SWEs (1.1).

2.1 Notations

Firstly, we divide the spatial domain $[a, b]$ into N uniform cells with $I_j = [x_{j-\frac{1}{2}}, x_{j+\frac{1}{2}}]$ for $j = 1, \dots, N$, where

$$a = x_{\frac{1}{2}} < x_{\frac{3}{2}} < \dots < x_{N+\frac{1}{2}} = b.$$

In addition, we denote the cell center and the uniform mesh size by $x_j = \frac{1}{2}(x_{j-\frac{1}{2}} + x_{j+\frac{1}{2}})$ and $\Delta x = \frac{b-a}{N}$, respectively. Under the framework of finite volume schemes, we look for numerical solution $\bar{U}_j(t)$ to approximate the cell average of the exact solution $U(x, t)$ on cell I_j , namely

$$\bar{U}(x_j, t) \approx \frac{1}{\Delta x} \int_{I_j} U(x, t) dx.$$

2.2 General formulation of the CWENO scheme

In this article, our semi-discrete finite volume CWENO scheme for the one-dimensional shallow water equations (1.2) enjoys the following form

$$\frac{d}{dt} \bar{U}_j(t) + \frac{1}{\Delta x} (\hat{F}_{j+\frac{1}{2}} - \hat{F}_{j-\frac{1}{2}}) = \frac{1}{\Delta x} \int_{I_j} S(U, b) dx. \quad (2.1)$$

Here, the notation $\hat{F}_{j+\frac{1}{2}} \triangleq \hat{f}(U_{j+\frac{1}{2}}^-, U_{j+\frac{1}{2}}^-)$ denote numerical fluxes and are used to approximate the physical fluxes at inter-cells, i.e., $F(U(x_{j+\frac{1}{2}}))$. The detailed construction of $\hat{F}_{j+\frac{1}{2}}$ will be described in Section 2.5.

2.3 A brief review of the CWENO reconstruction

Within the context of finite volume schemes, we only have cell averages at hands at each time level. To construct numerical fluxes and approximate the source term, we need values at inter-cells as well as values at the inner point of a cell for the usage of quadrature rules with high-order accuracy. Therefore, we need to employ reconstruction procedures to get the above values. Among them, the traditional WENO reconstruction is very successful and allows us to construct high-order WENO schemes (see [36–39] and references therein). However, the WENO reconstruction procedure has few shortcomings.

- Firstly, the linear weights d_k depend explicitly on the location of $\hat{x} \in I_j$.
- The computation of linear and nonlinear weights is required at different points on the inter-cells.
- In particular, in the case of the SWEs with the source term, more reconstruction procedures are needed to approximate the cell average of the source term.
- Moreover, for interior points, the linear weights may not exist (e.g., third-order WENO reconstruction at cell centre) or be non-positive (e.g., fifth-order WENO reconstruction at cell centre).

In this article, we apply the CWENO reconstruction procedure [40]. This CWENO reconstruction procedure can provide an entire reconstruction polynomial defined everywhere in a given cell and is especially convenient for the evaluation of the geometric

source term. In the following, we first present a brief review of the CWENO reconstruction operator.

Fixing a stencil $\{I_{j-r}, \dots, I_{j+r}\}$ involving $2r+1$ cell averages $\bar{u}_{j-r}, \dots, \bar{u}_{j+r}$, we need to obtain the reconstruction value at point $\hat{x} \in I_j$ with the help of the CWENO reconstruction. The specific steps of the CWENO reconstruction are as follows:

- 1) Firstly, we can get a polynomial of degree $2r$ denoted by $P_{\text{opt}}(x)$ based on the $2r+1$ cell averages $\bar{u}_{j-r}, \dots, \bar{u}_{j+r}$.
- 2) Secondly, we obtain a set of lower order polynomials $P_l(x) \in \mathbb{P}^r$ for $l=1, 2, \dots, r+1$.
- 3) Thirdly, we get a polynomial $P_0(x)$ defined as

$$P_0(x) = \frac{1}{d_0} \left(P_{\text{opt}}(x) - \sum_{l=1}^{r+1} d_l P_l(x) \right) \in \mathbb{P}^{2r}.$$

- 4) By means of the above reconstruction polynomials, the point value $\mathcal{R}_j(\hat{x})$ is given by the CWENO reconstruction operator in the below form

$$\mathcal{R}_j(\hat{x}) = \mathcal{R} \left(\hat{x}; \{\bar{u}_k\}_{k \in S_j} \right) = \sum_{l=0}^{r+1} \omega_l(\hat{x}) \cdot P_l(\hat{x}) \in \mathbb{P}^{2r}, \quad \hat{x} \in I_j. \tag{2.2}$$

The nonlinear weights ω_k in (2.2) are computed from the linear ones d_k as

$$\omega_l = \alpha_k \left(\sum_{i=0}^{r+1} \alpha_i \right)^{-1} \quad \text{based on} \quad \alpha_l = \frac{d_l}{(\beta_l + \epsilon)^2} \quad \text{for } l=0, 1, \dots, r+1,$$

where β_l denotes a suitable smoothness indicator, such as in [36], evaluated on the polynomial P_l in the cell I_j . Here, the parameter ϵ is a small positive quantity used here to avoid denominators being zero. In general, we take $\epsilon = 10^{-6}$ as in [36]. For more details, we refer to the reviews [37–39] for more details.

To determine the nonlinear weights ω_l , we must obtain the linear weights d_l in advance. First, we determine the temporary linear weights

$$\tilde{d}_l = \tilde{d}_{r+1-l} = l \quad \text{for } 1 \leq k \leq \frac{r+1}{2}.$$

In addition, we choose the linear coefficient $d_0 \in (0, 1)$ for the high-order polynomial $P_0(x)$. When d_0 is fixed, the final nonlinear weights are given by

$$d_l = \tilde{d}_l \left(\sum_{i=1}^{r+1} \tilde{d}_i \right)^{-1} (1 - d_0), \quad l=1, 2, \dots, r+1.$$

Remark 2.1. In particular, the parameter d_0 must satisfy $0 < d_0 < 1$. In fact, when d_0 is too close to 0 the polynomial $P_0(x)$ becomes unbounded. On the other hand, when d_0 is close to 1, the final reconstruction polynomial $\mathcal{R}_j(x)$ will almost coincide with the polynomial $P_{\text{opt}}(x)$, irrespectively of the oscillation indicators. In this article, we will take $d_0 = \frac{1}{2}$ as in [40].

Remark 2.2. Note that the polynomial $P_0(x) \in \mathbb{P}^{2r}$ is part of the reconstruction. The resulting CWENO reconstruction provides a polynomial $\mathcal{R}_j(x)$ that can be evaluated at any point within the cell I_j . In addition, the linear weights d_k are not needed to guarantee the accuracy of the reconstruction in smooth regions and can be chosen rather arbitrarily. Moreover, all the nonlinear weights ω_k involved in the reconstruction do not depend on particular points where the reconstruction is needed. The above observations are significant characteristics of the CWENO reconstruction different from the traditional WENO reconstruction [37–39].

2.4 The decomposition algorithm

Herein, based on the cell averages $\{\bar{U}\}_{j=1}^N$ at hands, we try to obtain the numerical solution in terms of the polynomial form denoted by $U(x)$ by means of the CWENO reconstruction. In addition, we also propose a novel decomposition algorithm for the reconstruction polynomial $U(x)$, which decomposes $U(x)$ into a reference equilibrium steady state $U^e(x)$ and a (possibly large) perturbation part $U^p(x)$ in terms of polynomials, namely

$$U(x) = U^e(x) + U^p(x).$$

This procedure is one of the key parts to construct the well-balanced scheme, and will be applied not only to the initial condition but also to the numerical solution at each time level. In the following, we will apply this algorithm in the process of construction of well-balanced numerical fluxes as well as discretizations to the source term.

In fact, due to the still water steady state solutions (1.3), we have

$$\bar{u}_j = 0, \quad \overline{(h+b)}_j = \text{Constant} \quad \text{for all } j. \quad (2.3)$$

Then, we define the equilibrium component of the water depth $h^e(x)$ in the cell I_j as follows

$$h_j^e(x) = (h+b)_j^{\text{CWENO}} - b(x), \quad x \in I_j. \quad (2.4)$$

Here, the notation $(h+b)_j^{\text{CWENO}}$ denotes the point value of the free surface level at the cell center x_j , which is obtained from the CWENO reconstruction. In this article, we assume that the bottom topography can be evaluated anywhere, either because it is a given function or obtained by a suitable interpolation.

Once $(h+b)_j^{\text{CWENO}}$ has been fixed, we can obtain the following equilibrium part of the numerical solution in cell I_j

$$U_j^e(x) = \begin{pmatrix} h_j^e(x) \\ (hu)_j^e(x) \end{pmatrix}, \quad x \in I_j, \tag{2.5}$$

with $(hu)_j^e(x) \equiv 0$ due to $u = 0$ at the steady state (1.3).

Next, the perturbation part $U_j^p(x)$ is obtained by applying the standard CWENO reconstruction \mathcal{R} in terms of the cell averages of the equilibrium perturbation and the numerical solution itself, namely

$$U_j^p(x) = \mathcal{R}_j \left(x; \left\{ \overline{U}_k - \overline{U}_k^e(x) \right\}_{k \in S_j} \right), \quad x \in I_j. \tag{2.6}$$

Note that the perturbation in cell I_k is obtained by taking a difference between the actual cell averages \overline{U}_k and the ones of the equilibrium part $U_k^e(x)$ in cells I_k neighbor to the given cell I_j . Here, the notation $\overline{U}_k^e(x)$ denotes the cell average of $U^e(x)$ using the $(2m-1)$ -th order accurate Gaussian quadrature rules in each cell I_k from the stencil of the cell I_j with the below form

$$\overline{U}_k^e(x) = \mathcal{Q}(U_k^e(x)) \triangleq \frac{1}{\Delta x} \sum_{l=1}^m \omega_l \cdot U_k^e(x_{k,l}), \quad k \in S_j, \tag{2.7}$$

with ω_l and $x_{k,l}$ being the weights and the nodes according to the cell I_k .

In the end, by means of adding the equilibrium part in (2.5) to the perturbation one in (2.6), we get a complete equilibrium preserving reconstruction denoted by \mathcal{W} , namely

$$U_j(x) = U_j^e(x) + U_j^p(x) \triangleq \mathcal{W}_j \left(x; \left\{ \overline{U}_k \right\}_{k \in S_j} \right), \quad x \in I_j. \tag{2.8}$$

2.5 Construction of well-balanced numerical fluxes

The construction of numerical fluxes

$$\widehat{F}_{j+\frac{1}{2}} = \widehat{f} \left(U_{j+\frac{1}{2}}^-, U_{j+\frac{1}{2}}^+ \right) \tag{2.9}$$

in (2.1) is the key element to achieve the final well-balanced scheme. Herein, we apply the following simple and efficient Lax-Friedrichs flux function

$$\widehat{f}(a_1, a_2) = \frac{1}{2} (F(a_1) + F(a_2) - \alpha(a_2 - a_1)), \tag{2.10}$$

with $\alpha = \max |u + \sqrt{gh}|$ being the maximum wave propagation speed over the whole spatial domain. In addition, the numerical flux function $\widehat{f}(\cdot, \cdot)$ in (2.10) satisfies the consistency, namely $\widehat{f}(u, u) = F(u)$.

Note that the inter-cells values $U_{j+\frac{1}{2}}^\pm$ used in (2.9) are obtained using the equilibrium preserving reconstruction (2.8) instead of the original reconstruction procedure (2.2).

To maintain the well-balanced property, our first priority is to ensure that for the still water steady state (1.3), the reconstructed values $U_{j+\frac{1}{2}}^\pm$ at inter-cells need to satisfy the below equalities

$$U_{j+\frac{1}{2}}^- = U_{j+\frac{1}{2}}^+ \triangleq U_{j+\frac{1}{2}}. \quad (2.11)$$

Consequently, in the case of the still water steady state (1.3), the numerical fluxes $\hat{F}_{j+\frac{1}{2}}$ reduce to the following form

$$\hat{F}_{j+\frac{1}{2}} = \hat{f}(U_{j+\frac{1}{2}}^-, U_{j+\frac{1}{2}}^+) = F(U_{j+\frac{1}{2}}) \quad (2.12)$$

due to the consistency of the Lax-Friedrichs flux function in (2.10). The realization of the above formula (2.12) is an important step to achieve the well-balanced property. Especially, in the process of constructing the well-balanced numerical fluxes, we are free of using the hydrostatic reconstruction as in [19, 24, 25, 31]. Similar technique has been used in [41].

2.6 The source term discretization

With the full equilibrium preserving reconstruction \mathcal{W} in (2.8) at hand, we propose a novel discretization for the source term by means of the decomposition algorithm in Section 2.4. We first split the water depth $h_j(x)$ into the equilibrium part $h_j^e(x)$ and the perturbation part $h_j^p(x)$ as follows

$$h_j(x) = h_j^e(x) + h_j^p(x), \quad x \in I_j.$$

Therefore, the momentum source term in the second equation can be rewritten as

$$\begin{aligned} S_j^{[2]}(x) &= -gh_j(x) \frac{db(x)}{dx} \\ &= -g \left(h_j^e(x) + h_j^p(x) \right) \frac{db(x)}{dx} \\ &= -gh_j^e(x) \frac{db(x)}{dx} - gh_j^p(x) \frac{db(x)}{dx}, \quad x \in I_j. \end{aligned} \quad (2.13)$$

However, a straightforward numerical integration for the above formula will not result in a well-balanced scheme. Herein, from the governing system (1.1), we observe the following equality

$$\frac{d\left(\frac{1}{2}g \left(h_j^e(x)\right)^2\right)}{dx} = -gh_j^e(x) \frac{db(x)}{dx}, \quad x \in I_j,$$

according to the equilibrium state (1.3).

Consequently, the original momentum source term in the second equation (2.13) can be written in the following formula equivalently

$$S_j^{[2]}(x) = \frac{d\left(\frac{1}{2}g\left(h_j^e(x)\right)^2\right)}{dx} - gh_j^p(x)\frac{db(x)}{dx}, \quad x \in I_j. \tag{2.14}$$

To integrate the two ends of the above formula at the same time in the cell I_j , we obtain the following equality

$$\begin{aligned} \frac{1}{\Delta x} \int_{I_j} S_j^{[2]}(x) dx &= \frac{\frac{1}{2}g\left(h^e\left(x_{j+\frac{1}{2}}\right)\right)^2 - \frac{1}{2}g\left(h^e\left(x_{j-\frac{1}{2}}\right)\right)^2}{\Delta x} \\ &\quad - \mathcal{Q}\left(g h_j^p(x)\frac{db(x)}{dx}\right), \quad x \in I_j. \end{aligned} \tag{2.15}$$

Here, we adopt the Gaussian quadrature rules for the second term in the right hand side of (2.15). The point values at the quadrature nodes in (2.15) are obtained using the CWENO reconstruction procedure.

2.7 The temporal discretization

On the premise of getting numerical fluxes as well as discretizations to the source term, the semi-discrete scheme (2.1) can be written out as an ODE

$$\frac{d}{dt} \bar{U}_j(t) = \mathcal{F}(\bar{U}) := -\frac{1}{\Delta x} \left(\hat{F}_{j+\frac{1}{2}} - \hat{F}_{j-\frac{1}{2}}\right) + \frac{1}{\Delta x} \int_{I_j} S(U, b) dx. \tag{2.16}$$

For the temporal discretization to the above ODE (2.16), we apply the third-order Runge-Kutta approach [42]

$$\bar{U}^{(1)} = \bar{U}^n + \Delta t \mathcal{F}(\bar{U}^n), \tag{2.17a}$$

$$\bar{U}^{(2)} = \frac{3}{4} \bar{U}^n + \frac{1}{4} \left(\bar{U}^{(1)} + \Delta t \mathcal{F}(\bar{U}^{(1)})\right), \tag{2.17b}$$

$$\bar{U}^{n+1} = \frac{1}{3} \bar{U}^n + \frac{2}{3} \left(\bar{U}^{(2)} + \Delta t \mathcal{F}(\bar{U}^{(2)})\right). \tag{2.17c}$$

2.8 Summary of the current scheme

The specific steps of the proposed scheme for the one-dimensional system (1.1) can be summarized as follows:

- (1) Initially, we obtain cell averages $\{\bar{U}_j\}_{j=1}^N$.
- (2) Split the numerical solution $U_j(x)$ into $U_j^e(x)$ and $U_j^p(x)$ using the full equilibrium preserving reconstruction \mathcal{W} in each cell I_j at each time level.

- (3) Construct well-balanced numerical fluxes $\widehat{F}_{j+\frac{1}{2}}$ through the formula (2.10).
- (4) Discretize the source term via the formula (2.15).
- (5) Get the semi-discrete scheme (2.16).
- (6) Update to the next time level by means of the Runge-Kutta approach (2.17).
- (7) Repeat the Steps (2)–(6).

2.9 Analysis of the well-balanced property

Here, we briefly summarize the well-balanced property and draw the below proposition.

Proposition 2.1. *The finite volume CWENO scheme (2.1), which is coupled with well-balanced numerical fluxes in (2.10), and a novel source term discretization in (2.15) using a Gaussian quadrature rule \mathcal{Q} as well as the full equilibrium preserving reconstruction \mathcal{W} in (2.8), is well-balanced for the still water steady state (1.3).*

Proof. The consistency and formal order of accuracy of the scheme is straightforward. In addition, at the still water steady state (1.3), in each cell $I_k \in I_j$, we have

$$\bar{U}_k = \overline{U_k^e(x)} = \mathcal{Q}(U_k^e(x)) \quad \text{for } k \in s_j,$$

which leads to the following perturbation part

$$U_j^p(x) = \mathcal{W}\left(x; \left\{ \bar{U}_k - \overline{U_k^e(x)} \right\}_{k \in s_j}\right) \equiv 0, \quad x \in I_j,$$

from (2.6).

Moreover, with the aid of the full equilibrium preserving reconstruction \mathcal{W} in (2.8), we get the water depth at inter-cells as follows

$$h\left(x_{j+\frac{1}{2}}^-\right) = h_j^e\left(x_{j+\frac{1}{2}}^-\right) + h_j^p\left(x_{j+\frac{1}{2}}^-\right) = (h+b)_j^{\text{CWENO}} - b\left(x_{j+\frac{1}{2}}\right), \quad (2.18a)$$

$$h\left(x_{j+\frac{1}{2}}^+\right) = h_{j+1}^e\left(x_{j+\frac{1}{2}}^+\right) + h_{j+1}^p\left(x_{j+\frac{1}{2}}^+\right) = (h+b)_{j+1}^{\text{CWENO}} - b\left(x_{j+\frac{1}{2}}\right). \quad (2.18b)$$

In addition, we observe the following fact that

$$(h+b)_j^{\text{CWENO}} = (h+b)_{j+1}^{\text{CWENO}} = \text{Constant},$$

by means of the reconstruction procedure. Then, we draw the below conclusion that

$$h\left(x_{j+\frac{1}{2}}^-\right) = h\left(x_{j+\frac{1}{2}}^+\right) \triangleq h^e\left(x_{j+\frac{1}{2}}\right),$$

due to the related operations in (2.18). Further, we also observe that

$$(hu)\left(x_{j+\frac{1}{2}}^-\right) = (hu)\left(x_{j+\frac{1}{2}}^+\right) = 0, \tag{2.19}$$

due to $(hu)^e(x) \equiv 0$.

In summary, we obtain the below equality

$$U_{j+\frac{1}{2}}^- = U_{j+\frac{1}{2}}^+ = \begin{pmatrix} h^e\left(x_{j+\frac{1}{2}}\right) \\ (hu)^e\left(x_{j+\frac{1}{2}}\right) \end{pmatrix} \triangleq \begin{pmatrix} h^e\left(x_{j+\frac{1}{2}}\right) \\ 0 \end{pmatrix}.$$

Hence, according to the consistency of the numerical flux function (2.10), we get

$$\begin{aligned} \hat{F}_{j-\frac{1}{2}} &= \hat{f}\left(U_{j-\frac{1}{2}}^-, U_{j-\frac{1}{2}}^+\right) = F\left(U_{j-\frac{1}{2}}^+\right) = \left(0, \frac{1}{2}g\left(h^e\left(x_{j-\frac{1}{2}}\right)\right)^2\right)^\top, \\ \hat{F}_{j+\frac{1}{2}} &= \hat{f}\left(U_{j+\frac{1}{2}}^-, U_{j+\frac{1}{2}}^+\right) = F\left(U_{j+\frac{1}{2}}^-\right) = \left(0, \frac{1}{2}g\left(h^e\left(x_{j+\frac{1}{2}}\right)\right)^2\right)^\top. \end{aligned}$$

Then, the discretization to the flux gradient reduces to the below equality

$$\frac{1}{\Delta x} \left(\hat{F}_{j+\frac{1}{2}}^{[2]} - \hat{F}_{j-\frac{1}{2}}^{[2]}\right) = \frac{\frac{1}{2}g\left(h^e\left(x_{j+\frac{1}{2}}\right)\right)^2 - \frac{1}{2}g\left(h^e\left(x_{j-\frac{1}{2}}\right)\right)^2}{\Delta x}. \tag{2.20}$$

Furthermore, at the steady state (1.3), the original discretization to the source term (2.15) reduces to the below form

$$\bar{S}_j^{[2]} = \frac{\frac{1}{2}g\left(h^e\left(x_{j+\frac{1}{2}}\right)\right)^2 - \frac{1}{2}g\left(h^e\left(x_{j-\frac{1}{2}}\right)\right)^2}{\Delta x}, \tag{2.21}$$

due to $U^p(x) \equiv 0$.

By plugging the above discretizations to the flux gradient (2.20) and to the source term (2.21) into the semi-discrete finite volume scheme (2.1), we get

$$\frac{d\bar{U}_j}{dt} = \mathcal{F}(\bar{U}) \triangleq -\frac{1}{\Delta x} \left(\hat{F}_{j+\frac{1}{2}} - \hat{F}_{j-\frac{1}{2}}\right) + \bar{S}_j \equiv 0.$$

Thus the scheme is well-balanced as claimed correspondingly. □

3 Extension to two-dimensional system

In this section, we extend the one-dimensional CWENO scheme to the following two-dimensional SWEs

$$h_t + (hu)_x + (hv)_y = 0, \tag{3.1a}$$

$$(hu)_t + \left(hu^2 + \frac{1}{2}gh^2\right)_x + (huv)_y = -ghb_x, \tag{3.1b}$$

$$(hv)_t + (huv)_x + \left(hv^2 + \frac{1}{2}gh^2\right)_y = -ghb_y, \tag{3.1c}$$

where v denotes the velocity in y -direction. In particular, the two-dimensional system maintains the below still water steady state solutions

$$u = v = 0, \quad h + b = \text{Constant}. \tag{3.2}$$

In a similar way, we rewrite this system (3.1) into the following compact form

$$U_t + F(U)_x + G(U)_y = S(U, b) \tag{3.3}$$

with

$$U = \begin{pmatrix} h \\ hu \\ hv \end{pmatrix}, \quad F(U) = \begin{pmatrix} hu \\ hu^2 + \frac{1}{2}gh^2 \\ huv \end{pmatrix},$$

$$G(U) = \begin{pmatrix} hv \\ huv \\ hv^2 + \frac{1}{2}gh^2 \end{pmatrix}, \quad S(U, b) = \begin{pmatrix} 0 \\ -ghb_x \\ -ghb_y \end{pmatrix}.$$

We deal with a rectangle computational domain $\Omega = [a, b] \times [c, d]$ discretized uniformly by N_x and N_y cells in x - and y -direction, respectively. The cells are labeled by $I_{i,j} = [x_{i-\frac{1}{2}}, x_{i+\frac{1}{2}}] \times [y_{j-\frac{1}{2}}, y_{j+\frac{1}{2}}]$ with $\Delta x = x_{i+\frac{1}{2}} - x_{i-\frac{1}{2}}$ and $\Delta y = y_{j+\frac{1}{2}} - y_{j-\frac{1}{2}}$ as cell sizes. A semi-discrete finite volume scheme for (3.3) enjoys the following form

$$\frac{d}{dt} \bar{U}_{i,j}(t) + \frac{1}{\Delta x} (\hat{F}_{i+\frac{1}{2},j} - \hat{F}_{i-\frac{1}{2},j}) + \frac{1}{\Delta y} (\hat{G}_{i,j+\frac{1}{2}} - \hat{G}_{i,j-\frac{1}{2}}) = \frac{1}{\Delta x \Delta y} \iint_{I_{i,j}} S(U, b) dx dy. \tag{3.4}$$

Here, the notation $\bar{U}_{i,j}(t)$ represents the cell averages of the conservative variables. In addition, $\hat{F}_{i+\frac{1}{2},j}$ and $\hat{G}_{i,j+\frac{1}{2}}$ denote numerical fluxes at inter-cells in the x - and y -direction, respectively. For the two-dimensional case, we also apply the Lax-Friedrichs numerical flux function (2.10) and the numerical fluxes $\hat{F}_{i+\frac{1}{2},j}$ and $\hat{G}_{i,j+\frac{1}{2}}$ enjoys the following forms

$$\hat{F}_{i+\frac{1}{2},j} = \frac{1}{2} (F(U_{i+\frac{1}{2},j}^-) + F(U_{i+\frac{1}{2},j}^+) - \alpha (U_{i+\frac{1}{2},j}^+ - U_{i+\frac{1}{2},j}^-)), \tag{3.5a}$$

$$\hat{G}_{i,j+\frac{1}{2}} = \frac{1}{2} (G(U_{i,j+\frac{1}{2}}^-) + G(U_{i,j+\frac{1}{2}}^+) - \alpha (U_{i,j+\frac{1}{2}}^+ - U_{i,j+\frac{1}{2}}^-)), \tag{3.5b}$$

with $\alpha = \max(|u + \sqrt{gh}|, |v + \sqrt{gh}|)$ as the maximum wave propagation speed over the whole computational domain.

To construct the above numerical fluxes and to achieve the source term approximation, we need to get $U_{i,j}(x, y)$ using reconstruction based on the cell averages. Herein, we apply the equilibrium preserving reconstruction similar to the one-dimensional case (2.8) with the below form

$$U_{i,j}(x, y) = U_{i,j}^e(x, y) + U_{i,j}^p(x, y) \triangleq \mathcal{W}_{i,j}(x, y; \{\bar{U}_{k,l}\}_{k,l \in S_{i,j}}), \quad (x, y) \in I_{i,j}. \tag{3.6}$$

Therefore, we can obtain the values at inter-cells, i.e., $U_{i+\frac{1}{2},j}^\pm$ and $U_{i,j+\frac{1}{2}}^\pm$. The equilibrium steady state part has the following form

$$U_{i,j}^e(x,y) = \begin{pmatrix} h_{i,j}^e(x,y) \\ (hu)_{i,j}^e(x,y) \\ (hv)_{i,j}^e(x,y) \end{pmatrix}, \quad (x,y) \in I_{i,j}, \tag{3.7}$$

with

$$(hu)_{i,j}^e(x,y) = (hv)_{i,j}^e(x,y) \equiv 0$$

due to $u = v = 0$ at the steady state (3.2). In particular, the equilibrium component of the water depth enjoys the below form

$$h_{i,j}^e(x,y) = (h+b)_{i,j}^{\text{CWENO}} - b(x,y), \quad (x,y) \in I_{i,j}. \tag{3.8}$$

Here, the notation $(h+b)_{i,j}^{\text{CWENO}}$ denotes the point value of the free surface level at the cell center, which is obtained from the CWENO reconstruction. Moreover, in analogy to the one-dimensional case, we can also get the perturbation part of the conservative variables with the below forms

$$U_{i,j}^p(x,y) = \mathcal{R}_{i,j} \left(x,y; \left\{ \bar{U}_{k,l} - \overline{U_{k,l}^e(x,y)} \right\}_{(k,l) \in S_{i,j}} \right), \quad (x,y) \in I_{i,j}.$$

In addition, the source term can be equivalently rewritten as follow

$$\begin{aligned} S_{i,j}^{[2]}(x,y) &= -gh_{i,j}(x,y) \frac{db(x,y)}{dx} \\ &= -gh_{i,j}^e(x,y) \frac{db(x,y)}{dx} - gh_{i,j}^p(x,y) \frac{db(x,y)}{dx}, \quad (x,y) \in I_{i,j}. \end{aligned} \tag{3.9a}$$

$$\begin{aligned} S_{i,j}^{[3]}(x,y) &= -gh_{i,j}(x,y) \frac{db(x,y)}{dy} \\ &= -gh_{i,j}^e(x,y) \frac{db(x,y)}{dy} - gh_{i,j}^p(x,y) \frac{db(x,y)}{dy}, \quad (x,y) \in I_{i,j}. \end{aligned} \tag{3.9b}$$

Subsequently, we approximate the source terms as follows

$$\begin{aligned} &\frac{1}{\Delta x \Delta y} \iint_{I_{i,j}} S_{i,j}^{[2]}(x,y) dx dy \\ &= \frac{1}{\Delta x \Delta y} \int_{y_{j-\frac{1}{2}}}^{y_{j+\frac{1}{2}}} \left(\frac{1}{2}g \left(h^e \left(x_{j+\frac{1}{2}}, y \right) \right)^2 - \frac{1}{2}g \left(h^e \left(x_{j-\frac{1}{2}}, y \right) \right)^2 \right) dy - \mathcal{Q} \left(gh_{i,j}^p(x,y) \frac{db(x,y)}{dx} \right), \end{aligned} \tag{3.10a}$$

$$\begin{aligned} &\frac{1}{\Delta x \Delta y} \iint_{I_{i,j}} S_{i,j}^{[3]}(x,y) dx dy \\ &= \frac{1}{\Delta x \Delta y} \int_{x_{i-\frac{1}{2}}}^{x_{i+\frac{1}{2}}} \left(\frac{1}{2}g \left(h^e \left(x, y_{j+\frac{1}{2}} \right) \right)^2 - \frac{1}{2}g \left(h^e \left(x, y_{j-\frac{1}{2}} \right) \right)^2 \right) dx - \mathcal{Q} \left(gh_{i,j}^p(x,y) \frac{db(x,y)}{dy} \right). \end{aligned} \tag{3.10b}$$

Herein, we employ the following Gaussian quadrature rules

$$\mathcal{Q}(c(x,y)) \triangleq \sum_{k=1}^m \sum_{l=1}^m \omega_k \omega_l c(x_{i,k}, y_{j,l}) \approx \frac{1}{\Delta x \Delta y} \iint_{I_{i,j}} c(x,y) dx dy.$$

4 Numerical results

In this section, we carry out extensive numerical examples to validate performance of the current scheme. To ensure the numerical stability for the one-dimensional problems, we adopt an adaptive time step Δt satisfying the following condition

$$\frac{\Delta t}{\Delta x} \max_i \left(|\bar{u}_i^n| + \sqrt{g \bar{h}_i^n} \right) = CFL$$

with CFL being the Courant-Friedrichs-Levy constant and set the CFL number as 0.6 except for special examples. With respect to the two-dimensional case, we adopt a similar CFL time restriction. In addition, we apply $(2r+1)$ -th order accurate CWENO reconstruction with $r=2$, and use $(2m-1)$ -th order accurate Gaussian quadrature rule with $m=3$. Therefore, the resulting scheme can achieve 5-th order accuracy for smooth solutions. In addition, for the two-dimensional problems, the time step should satisfy the following condition

$$\Delta t \left(\frac{\max_{i,j} (|\bar{u}_{ij}^n| + \sqrt{g \bar{h}_{ij}^n})}{\Delta x} + \frac{\max_{i,j} (|\bar{v}_{ij}^n| + \sqrt{g \bar{h}_{ij}^n})}{\Delta y} \right) = CFL.$$

4.1 One-dimensional system

4.1.1 Testing the well-balanced property

To testify the well-balanced property, we handle an example from [12] with the following initial conditions

$$u = 0 \text{ m/s} \quad \text{and} \quad h + b = 10 \text{ m}$$

on $[0, 10] \text{ m}$. Here, we consider two different bottom topographies, the first one is smooth

$$b(x) = 5 \exp \left(-\frac{2}{5} (x-5)^2 \right) \text{ m},$$

and the second one is discontinuous

$$b(x) = \begin{cases} 4 \text{ m}, & \text{if } 4 \leq x \leq 8 \text{ m}, \\ 0 \text{ m}, & \text{otherwise.} \end{cases}$$

Then, we calculate the numerical errors of the solutions between at $t = 0 \text{ s}$ and at $t = 0.5 \text{ s}$ and present them in Tables 1 and 2, respectively. The errors are all at the level of

Table 1: Numerical errors of the example over a smooth bottom.

Precision	L^1 error		L^2 error		L^∞ error	
	h	hu	h	hu	h	hu
Single	3.6571E-07	3.6190E-07	4.1269E-07	4.2761E-07	3.3329E-07	3.5081E-07
Double	4.4182E-14	4.2908E-14	4.0293E-14	4.0932E-14	4.2908E-14	3.0286E-14

Table 2: Numerical errors of the example over a discontinuous bottom.

Precision	L^1 error		L^2 error		L^∞ error	
	h	hu	h	hu	h	hu
Single	2.6042E-07	4.2094E-07	5.3096E-07	3.5096E-07	3.0736E-07	3.2908E-07
Double	4.5309E-14	5.0285E-13	5.3301E-14	4.4903E-13	5.2493E-13	4.0096E-13

the machine accuracy; the expected well-balanced property is achieved correspondingly. Therefore, from the numerical point of view, the one-dimensional CWENO scheme is a well-balanced one.

4.1.2 Testing the orders of accuracy

To testify the orders of accuracy, we adopt an example from [12] with the following bottom as well as initial data

$$\begin{aligned}
 b(x) &= \sin^2(\pi x)m, \\
 h(x,0) &= (5 + \exp(\cos(2\pi x)))m, \\
 (hu)(x,0) &= \sin(\cos(2\pi x))m^2/s,
 \end{aligned}$$

on a unit spatial domain $[0,1]m$.

Because the exact solutions are not available, we firstly compute this example up to $t = 0.1s$ on a very refined mesh with 12,800 cells and take the obtained solutions as the reference ones. Subsequently, by means of the obtained reference solutions, we calculate the L^1 errors at $t = 0.1s$ and the accuracy orders based on different meshes, then illustrate them in Table 3. The expected fifth-order accuracy is clearly achieved.

4.1.3 Perturbations of a steady state water flow

This example is used here to testify the ability of the current scheme to capture small perturbations to the steady state [43]. We consider a bottom of a bump shape

$$b(x) = \begin{cases} 0.25(\cos(10\pi(x-1.5))+1)m, & \text{if } 1.4 \leq x \leq 1.6m, \\ 0m, & \text{otherwise,} \end{cases}$$

on a spatial $[0,2]m$. The initial conditions are regarded as a small perturbation to the steady state solutions with the below form

$$h(x,0) = \begin{cases} (1-b(x)+\epsilon)m, & \text{if } 1.1 \leq x \leq 1.2m, \\ (1-b(x))m, & \text{otherwise,} \end{cases} \quad \text{and} \quad u(x,0) = 0m/s,$$

Table 3: L^1 errors and orders of accuracy for the example in Section 4.1.2.

Cells	h		hu	
	L^1 error	Order	L^1 error	Order
10	4.3958E-02		5.2307E-02	
20	8.0448E-03	2.45	9.6393E-03	2.44
40	8.7542E-04	3.20	1.0417E-03	3.21
80	6.3287E-05	3.79	7.4787E-05	3.80
160	2.5207E-06	4.65	3.0204E-06	4.63
320	8.9240E-08	4.82	1.0842E-07	4.80
640	2.7692E-09	5.01	3.3882E-09	5.00

with $\epsilon > 0$ a parameter. Herein, we handle two different cases: $\epsilon = 0.2\text{m}$ for a big pulse and $\epsilon = 0.001\text{m}$ for a small pulse, separately.

As time develops, the initial perturbation breaks up into two pulses moving in different directions, which are shown in Fig. 1 and Fig. 2 at $t = 0.2\text{s}$ on a mesh with 200 cells. Although on a relative coarse mesh, the two pulses are all well resolved and are in perfect agreement with those in the literature [12, 43, 44].

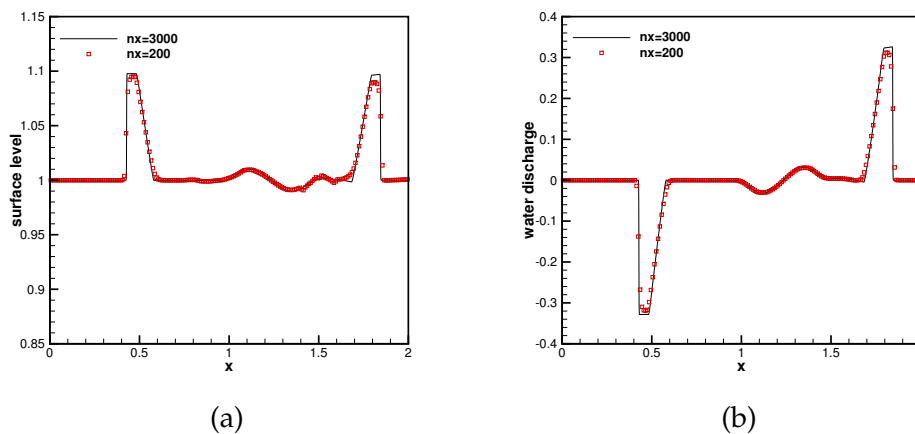


Figure 1: Free surface level $h+b$ (a) and water discharge hu (b) of the big pulse example in Section 4.1.3 at $t = 0.2\text{s}$.

4.1.4 The dam break problem over a rectangular bump

Then, we numerically simulate a dam break problem from [10, 12, 17, 44], and employ the below initial data

$$h(x,0) = \begin{cases} (20-b(x))\text{m}, & \text{if } x \leq 750\text{m}, \\ (15-b(x))\text{m}, & \text{otherwise,} \end{cases} \quad \text{and} \quad u(x,0) = 0\text{m/s},$$

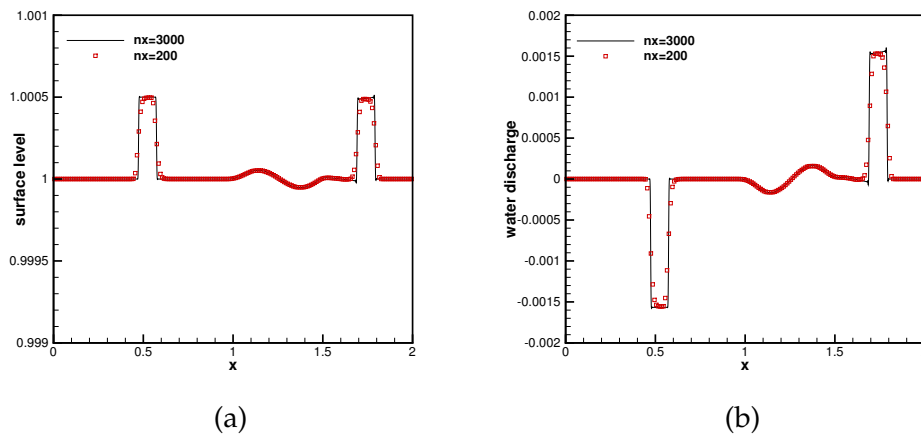


Figure 2: Free surface level $h+b$ (a) and water discharge hu (b) of the small pulse example in Section 4.1.3 at $t=0.2s$.

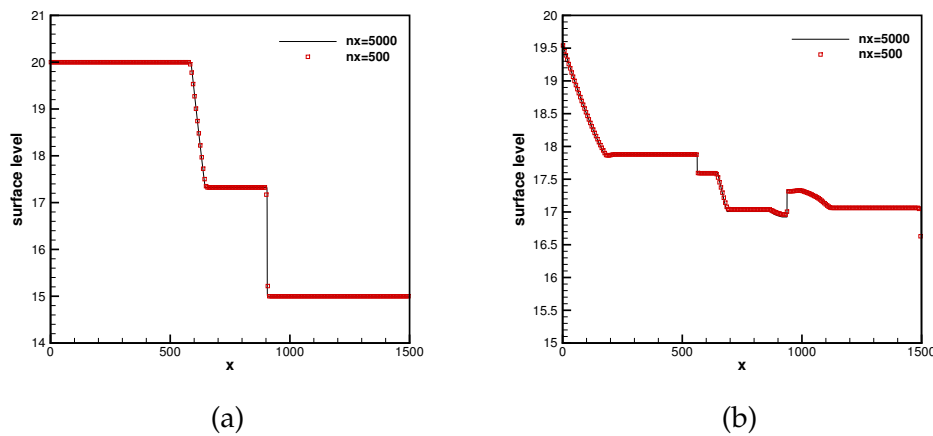


Figure 3: Free surface level $h+b$ of the example in Section 4.1.4 at $t=15s$ (a) and $t=60s$ (b).

over a rectangular like bottom topography

$$b(x) = \begin{cases} 8m, & \text{if } |x-750| \leq 1500/8m, \\ 0m, & \text{otherwise,} \end{cases}$$

on a spatial domain $[0,1500]m$.

We present the numerical results at $t=15s$ and at $t=60s$ in Fig. 3. From Fig. 3, we can observe that the current scheme performs well and produces well resolved, non-oscillatory numerical results, which are in good agreement with the reference ones. Moreover, the numerical results here are comparable with those in the literature [10,12,17,44].

4.1.5 Steady flow over a hump

Further, we implement a classical example from [45] to validate the proposed scheme. This example includes transcritical and subcritical flows and is widely used to testify well-balanced schemes. The initial data are given by

$$h(x,0) = 0.33\text{m} \quad \text{and} \quad u(x,0) = 0\text{m/s}$$

over a hump

$$b(x) = \begin{cases} (0.2 - 0.05(x-10)^2)\text{m}, & \text{if } 8 \leq x \leq 12\text{m}, \\ 0\text{m}, & \text{otherwise,} \end{cases}$$

on a spatial domain $[0,25]\text{m}$. Then, we solve this example on a mesh with 200 cells until $t = 200\text{s}$ and impose different boundary conditions. To have a better comparison, we also present the exact solutions obtained from [46].

Case A: the transcritical flow without a shock. A discharge $hu = 1.53\text{m}^2/\text{s}$ and a water depth $h = 0.66\text{m}$ are imposed at the upstream boundary and on the downstream one, respectively. The numerical results are in good agreement with the exact ones, see Fig. 4.

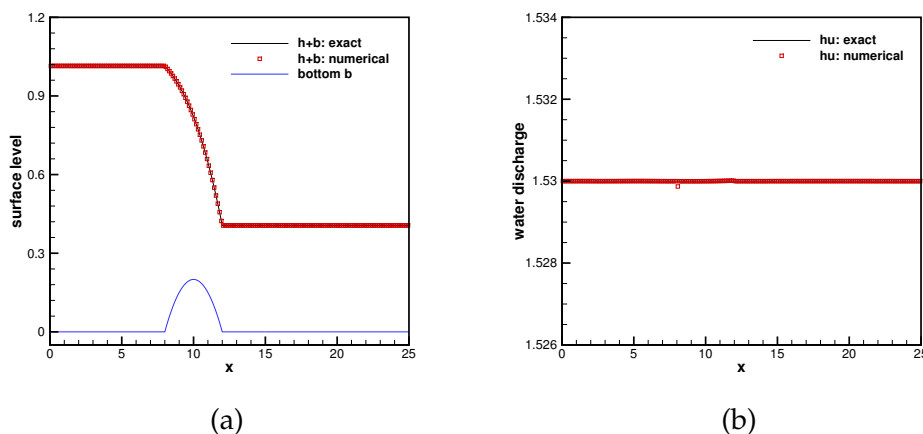


Figure 4: Free surface level $h+b$ (a) and water discharge hu (b) of the Case A in Section 4.1.5 at $t = 200\text{s}$.

Case B: the transcritical flow with a shock. A water discharge $hu = 0.18\text{m}^2/\text{s}$ and a water depth $h = 0.33\text{m}$ are imposed on the upstream boundary and on the downstream one, respectively. The numerical results in Fig. 5 are in good agreement with the exact ones and are free of spurious oscillations.

Case C: the subcritical flow. Here, we exert a water discharge $hu = 4.42\text{m}^2/\text{s}$ and a water depth $h = 2\text{m}$ on the upstream boundary and on the downstream one, respectively. Numerical solutions together with the exact solutions are shown in Fig. 6; the numerical solutions and the exact ones fit very well.

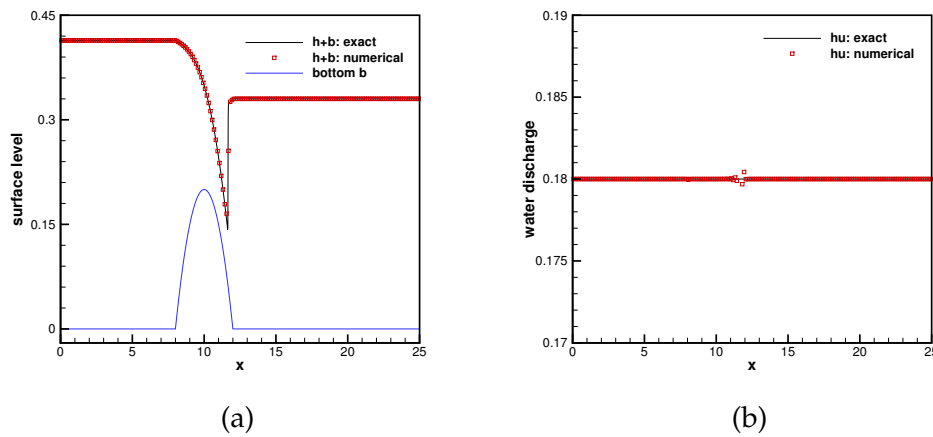


Figure 5: Free surface level $h+b$ (a) and water discharge hu (b) of the Case B in Section 4.1.5 at $t=200s$.

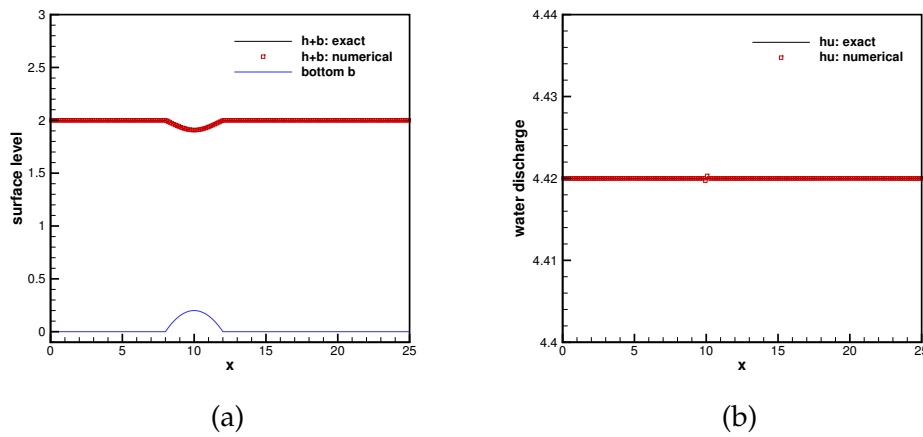


Figure 6: Free surface level $h+b$ (a) and water discharge hu (b) of the Case C in Section 4.1.5 at $t=200s$.

4.1.6 The tidal wave flow

Subsequently, we deal with an example from [47] with the following initial data

$$h(x,0) = (60.5 - b(x))m,$$

$$hu(x,0) = 0m^2/s,$$

on the below bottom topography

$$b(x) = \left(10 + \frac{40x}{L} + 10\sin\left(\pi\left(\frac{4x}{L} - \frac{1}{2}\right)\right) \right) m,$$

with $L = 14000m$ being the length of the spatial domain.

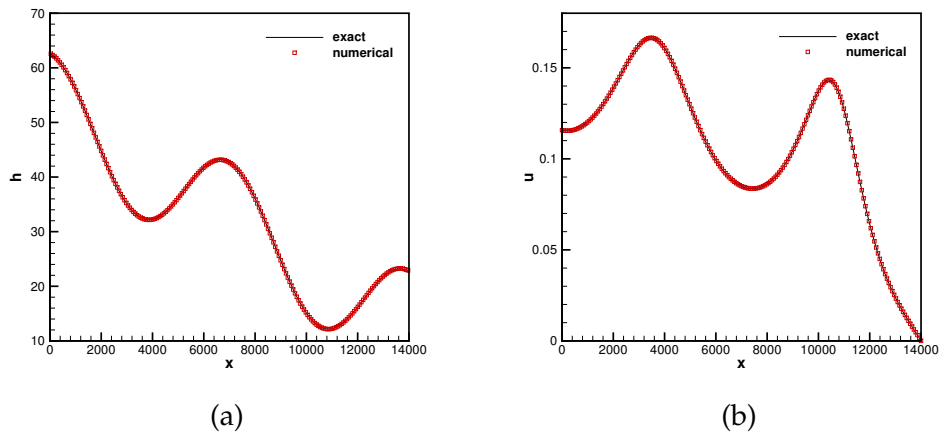


Figure 7: Water depth h (a) and flow velocity u (b) of the example in Section 4.1.6 at $t = 7552.13$ s.

We impose the below boundary conditions

$$h(0,t) = \left(64.5 - 4 \sin \left(\pi \left(\frac{4t}{86400} + \frac{1}{2} \right) \right) \right) \text{m},$$

$$hu(L,t) = 0 \text{m}^2/\text{s},$$

at both ends of the spatial domain. Moreover, we also employ the exact solutions

$$h(x,t) = \left(64.5 - b(x) - 4 \sin \left(\pi \left(\frac{4t}{86400} + \frac{1}{2} \right) \right) \right) \text{m},$$

$$(hu)(x,t) = \frac{(x-L)\pi}{5400} \cos \left(\pi \left(\frac{4t}{86400} + \frac{1}{2} \right) \right) \text{m}^2/\text{s},$$

from [47] for the sake of comparison.

We present the water depth h and the flow velocity u on a mesh with 200 cells at $t = 7552.13$ s in Fig. 7. The numerical results are obviously consistent with the exact ones even for a long time simulation. This observation strongly suggests that the proposed scheme is very suitable for numerical simulation with long time.

4.2 Two-dimensional system

In the following, we deal with the two-dimensional numerical examples.

4.2.1 Testing the well-balanced property

Here, we implement an example from [12] along with the following initial data as well as the bottom

$$\begin{aligned} h(x,y,0) &= (1-b(x,y))m, \\ u(x,y,0) &= v(x,y,0) = 0m/s, \\ b(x,y) &= 0.8\exp(-50((x-0.5)^2+(y-0.5)^2))m, \end{aligned}$$

on a unit spatial domain $[0,1]m \times [0,1]m$.

Then, we calculate L^1 errors between the initial solutions at $t=0s$ and the numerical ones at $t=0.1s$ on a mesh with 100×100 cells, and then present the L^1 errors in Table 4. It is clear that the numerical errors are all at the level of the machine accuracy even for different precisions; this observation strongly suggests that the current scheme maintains the well-balanced property even for the two-dimensional system.

Table 4: L^1 errors with different precisions for the still water steady state solutions.

Precision	L^1 error		
	h	hu	hv
Single	2.85×10^{-7}	4.91×10^{-7}	3.34×10^{-7}
Double	5.37×10^{-14}	4.49×10^{-14}	4.07×10^{-14}

4.2.2 A small perturbation of a two-dimensional steady state water flow

This test case is originally developed by LeVeque [43] and has been widely used to validate well-balanced schemes near the vicinity of a steady state, see [12, 16, 17, 20, 44]. The initial data can be taken as a small perturbation of a steady state with the following form

$$\begin{aligned} h(x,y,0) &= \begin{cases} (1-b(x,y)+0.01)m, & \text{if } 0.05 \leq x \leq 0.15m, \\ (1-b(x,y))m, & \text{otherwise,} \end{cases} \\ u(x,y,0) &= v(x,y,0) = 0m/s, \end{aligned}$$

over an elliptical like bottom

$$b(x,y) = 0.8\exp(-5(x-0.9)^2-50(y-0.5)^2)m$$

on a spatial domain $[0,2]m \times [0,1]m$.

We implement this example on two different meshes with rectangular cells for the sake of comparison and illustrate the contours of the free surface level $h+b$ in Fig. 8. The proposed scheme obviously resolves complex features of the flow very well even on relatively coarse meshes. Furthermore, the numerical results here can be compared with those in the literature [12, 16, 17, 20, 44].

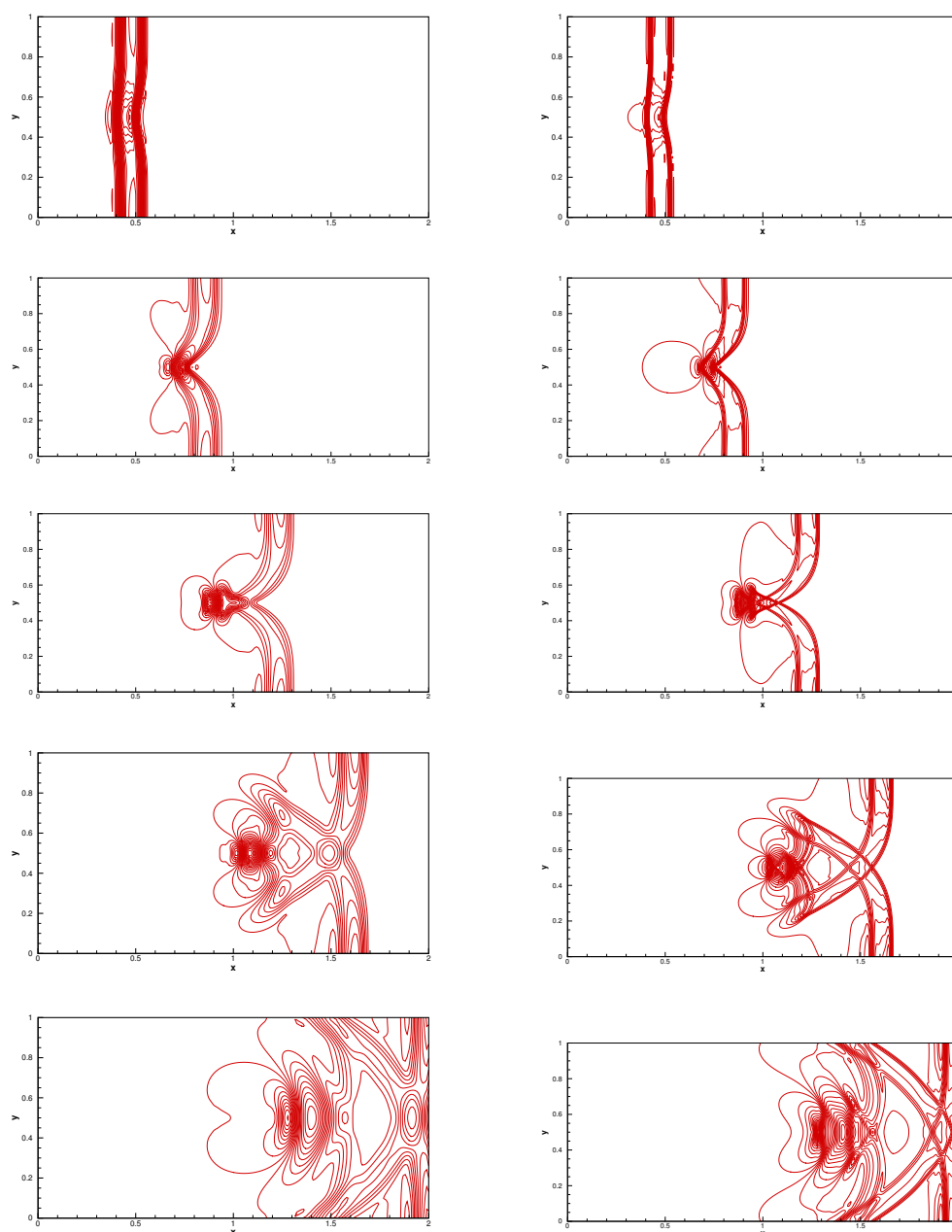


Figure 8: Thirty contours of free surface level $h+b$ of the example in Section 4.2.2. From top to bottom: at $t=0.12$ s from 0.99942 m to 1.00656 m; at $t=0.24$ s from 0.99318 m to 1.01659 m; at $t=0.36$ s from 0.98814 m to 1.01161 m; at $t=0.48$ s from 0.99023 m to 1.00508 m; and at $t=0.6$ s from 0.99514 m to 1.00629 m. Left: 200×100 cells. Right: 600×300 cells.

5 Conclusions

In this article, we develop a new well-balanced finite volume CWENO scheme for one- and two-dimensional shallow water equations with the geometrical source term. With

the help of the CWENO reconstruction, we achieve a novel equilibrium preserving reconstruction, which leads to a decomposition algorithm. By means of the decomposition algorithm, we can easily construct well-balanced numerical fluxes and avoid applying the traditional hydrostatic reconstruction technique. Moreover, this decomposition algorithm also helps us realize a simple source term discretization, which is consistent with the discretization to the flux gradient. Therefore, we finally realize a well-balanced finite volume scheme. Rigorous theoretical analysis and extensive numerical examples all verify the resulting well-balanced property. Furthermore, numerical results strongly imply that the proposed scheme keeps high-order accuracy for smooth solutions, and enjoys good resolutions for discontinuous solutions at the same time.

Acknowledgements

The third author Shouguo Qian is supported by the Natural Science Foundation of Shandong Province (Grant No. ZR2021MA072). The author Gang Li is supported by the Natural Science Foundation of China (Grant No. 11771228). The author Qiang Niu is supported by the Qinglan Project of Jiangsu Province, the XJTLU research enhancement fund (No. REF-18-01-04) and the Key Programme Special Fund (KSF) in XJTLU (Nos. KSF-E-32 and KSF-E-21).

References

- [1] S. F. BRADFORD AND B. F. SANDERS, *Finite volume model for shallow water flooding of arbitrary topography*, J. Hydraulic Eng., 128(3) (2002), pp. 289–298.
- [2] G. GOTTARDI AND M. VENUTELLI, *Central scheme for the two-dimensional dam-break flow simulation*, Adv. Water Res., 27 (2004), pp. 259–268.
- [3] C. B. VREUGDENHIL, *Numerical Methods for Shallow-Water Flow*, Springer, Dordrecht, 15-25, 1995.
- [4] J. M. GREENBERG AND A. Y. LEROUX, *A well-balanced scheme for the numerical processing of source terms in hyperbolic equations*, SIAM J. Numer. Anal., 33 (1996), pp. 1–16.
- [5] J. M. GREENBERG, A. Y. LEROUX, R. BARAILLE AND A. NOUSSAIR, *Analysis and approximation of conservation laws with source terms*, SIAM J. Numer. Anal., 34 (1997), pp. 1980–2007.
- [6] S. NOELLE, Y. L. XING AND C.-W. SHU, *High-order well-balanced schemes*, in: Numerical Methods for Balance Laws, (G. Puppo and G. Russo eds), Quaderni di Matematica, 2010.
- [7] B. PERTHAME AND C. SIMEONI, *A kinetic scheme for the Saint-Venant system with a source term*, Calcolo, 38 (2001), pp. 201–231.
- [8] K. XU, *A well-balanced gas-kinetic scheme for the shallow-water equations with source terms*, J. Comput. Phys., 178 (2002), pp. 533–562.
- [9] A. KURGANOV AND D. LEVY, *Central-upwind schemes for the Saint-Venant system*, Math. Model. Numer. Anal., 36 (2002), pp. 397–425.
- [10] S. VUKOVIC AND L. SOPTA, *ENO and WENO schemes with the exact conservation property for one-dimensional shallow water equations*, J. Comput. Phys., 179 (2002), pp. 593–621.

- [11] S. VUKOVIC, N. CRNJARIC-ZIC AND L. SOPTA, *WENO schemes for balance laws with spatially varying flux*, J. Comput. Phys., 199 (2004), pp. 87–109.
- [12] Y. L. XING AND C.-W. SHU, *High order finite difference WENO schemes with the exact conservation property for the shallow water equations*, J. Comput. Phys., 208 (2005), pp. 206–227.
- [13] S. NOELLE, N. PANKRATZ, G. PUPPO AND J. NATVIG, *Well-balanced finite volume schemes of arbitrary order of accuracy for shallow water flows*, J. Comput. Phys., 213 (2006), pp. 474–499.
- [14] Y. L. XING AND C.-W. SHU, *High order well-balanced finite volume WENO schemes and discontinuous Galerkin methods for a class of hyperbolic systems with source terms*, J. Comput. Phys., 214 (2006), pp. 567–598.
- [15] S. NOELLE, Y. XING AND C.-W. SHU, *High-order well-balanced finite volume WENO schemes for shallow water equation with moving water*, J. Comput. Phys., 226(1) (2007), pp. 29–58.
- [16] G. LI, C. LU AND J. QIU, *Hybrid well-balanced WENO schemes with different indicators for shallow water equations*, J. Sci. Comput., 51 (2012), pp. 527–559.
- [17] G. LI, V. CALEFFI AND Z. K. QI, *A well-balanced finite difference WENO scheme for shallow water flow model*, Appl. Math. Comput., 265 (2015), pp. 1–16.
- [18] Q. ZHU, Z. GAO, W. S. DON AND X. Q. LV, *Well-balanced hybrid compact-WENO scheme for shallow water equations*, Appl. Numer. Math., 112 (2017), pp. 65–78.
- [19] J. J. LI, G. LI, S. G. QIAN AND J. M. GAO, *High-order well-balanced finite volume WENO schemes with conservative variables decomposition for shallow water equations*, Adv. Appl. Math. Mech., 13 (2021), pp. 827–849.
- [20] V. CALEFFI, *A new well-balanced Hermite weighted essentially non-oscillatory scheme for shallow water equations*, Int. J. Numer. Methods Fluids, 67 (2011), pp. 1135–1159.
- [21] G. RUSSO, *Central schemes for balance laws*, in: Proceedings of the VIII International Conference on Nonlinear Hyperbolic Problems, Magdeburg, 2000.
- [22] R. TOUMA AND S. KHANKAN, *Well-balanced unstaggered central schemes for one and two-dimensional shallow water equation systems*, Appl. Math. Comput., 218 (2012), pp. 5948–5960.
- [23] A. ERN, S. PIPERNO AND K. DJADEL, *A well-balanced Runge-Kutta discontinuous Galerkin method for the shallow-water equations with flooding and drying*, Int. J. Numer. Methods Fluids, 58 (2008), pp. 1–25.
- [24] Y. L. XING, *Exactly well-balanced discontinuous Galerkin methods for the shallow water equations with moving water equilibrium*, J. Comput. Phys., 257 (2014), pp. 536–553.
- [25] G. LI, L. N. SONG AND J. M. GAO, *High order well-balanced discontinuous Galerkin methods based on hydrostatic reconstruction for shallow water equations*, J. Comput. Appl. Math., 340 (2018), pp. 546–560.
- [26] G. VIGNOLI, V. A. TITAREV AND E. F. TORO, *ADER schemes for the shallow water equations in channel with irregular bottom elevation*, J. Comput. Phys., 227 (2008), pp. 2463–2480.
- [27] A. NAVAS-MONTILLA AND J. MURILLO, *Energy balanced numerical schemes with very high order. The Augmented Roe Flux ADER scheme. Application to the shallow water equations*, J. Comput. Phys., 290 (2015), pp. 188–218.
- [28] G. J. GASSNER, A. R. WINTERS AND D. A. KOPRIVA, *A well balanced and entropy conservative discontinuous Galerkin spectral element method for the shallow water equations*, Appl. Math. Comput., 272 (2016), pp. 291–308.
- [29] C. BERTHON AND C. CHALONS, *A fully well-balanced, positive and entropy-satisfying Godunov-type method for the shallow-water equations*, Math. Comput., 85 (2016), pp. 1281–1307.
- [30] X. H. YUAN, *A well-balanced element-free Galerkin method for the nonlinear shallow water equations*, Appl. Math. Comput., 331 (2018), pp. 46–53.
- [31] G. LI, J. J. LI, S. G. QIAN AND J. M. GAO, *A well-balanced ADER discontinuous Galerkin*

- method based on differential transformation procedure for shallow water equations*, Appl. Math. Comput., 395 (2021), p. 125848.
- [32] L. GOSSE, *Computing Qualitatively Correct Approximations of Balance Laws*, Springer, Milan, 2013.
- [33] F. BOUCHUT, *Nonlinear Stability of Finite Volume Methods for Hyperbolic Conservation Laws*, Birkhäuser Basel, Springer, 2004.
- [34] Y. L. XING AND C.-W. SHU, *A survey of high order schemes for the shallow water equations*, J. Math. Study, 47 (2014), pp. 221–249.
- [35] E. AUDUSSE, F. BOUCHUT, M. O. BRISTEAU, R. KLEIN AND B. PERTHAME, *A fast and stable well-balanced scheme with hydrostatic reconstruction for shallow water flows*, SIAM J. Sci. Comput., 25 (2004), pp. 2050–2065.
- [36] G. S. JIANG AND C.-W. SHU, *Efficient implementation of weighted ENO schemes*, J. Comput. Phys., 126 (1996), pp. 202–228.
- [37] C.-W. SHU, *Essentially non-oscillatory and weighted essentially non-oscillatory schemes for hyperbolic conservation laws*, NASA/CR-97-206253, ICASE Report, NO.97-65, 1997.
- [38] C.-W. SHU, *High order weighted essentially nonoscillatory schemes for convection dominated problems*, SIAM Rev., 51 (2009), pp. 82–126.
- [39] C.-W. SHU, *High order WENO and DG methods for time-dependent convection-dominated PDEs: A brief survey of several recent developments*, J. Comput. Phys., 316 (2016), pp. 598–613.
- [40] I. CRAVERO, G. PUPPO, M. SEMPLICE AND G. VISCONTI, *CWENO: Uniformly accurate reconstructions for balance laws*, Math. Comput., 87 (2017), pp. 1689–1719.
- [41] M. S. JIANG, Z. Y. ZHANG AND J. ZHAO, *Improving the accuracy and consistency of the scalar auxiliary variable (SAV) method with relaxation*, J. Comput. Phys., 456 (2022), p. 110954.
- [42] C.-W. SHU AND S. OSHER, *Efficient implementation of essentially non-oscillatory shock-capturing schemes*, J. Comput. Phys., 77 (1998), pp. 439–471.
- [43] R. J. LEVEQUE, *Balancing source terms and flux gradient on high-resolution Godunov methods: the quasi-steady wave-propagation algorithm*, J. Comput. Phys., 146 (1998), pp. 346–365.
- [44] Y. L. XING AND C.-W. SHU, *A new approach of high order well-balanced finite volume WENO schemes and discontinuous Galerkin methods for a class of hyperbolic systems with source terms*, Commun. Comput. Phys., 1 (2006), pp. 100–134.
- [45] M. E. VAZQUEZ-CENDON, *Improved treatment of source terms in upwind schemes for the shallow water equations in channels with irregular geometry*, J. Comput. Phys., 148 (1999), pp. 497–526.
- [46] N. GOUTAL AND F. MAUREL, *Proceedings of the second workshop on Dam-Break wave simulation*, Technical Report HE-43/97/016/A, Electricité de France, Département Laboratoire National d’Hydraulique, Groupe Hydraulique Fluviale, 1997.
- [47] A. BERMUDEZ AND M. E. VAZQUEZ, *Upwind methods for hyperbolic conservation laws with source terms*, Comput. Fluids, 23 (1994), pp. 1049–1071.